43. R. E. M. Rickaby, H. Elderfield, *Geochem. Geophys. Geosyst.* **6**, Q05001 10.1029/2004GC000858 (2005).
44. F. Lamy *et al.*, *Earth Planet. Sci. Lett.* **259**, 400 (2007).
45. J. E. Tierney, J. M. Russell, *Geophys. Res. Lett.* **34**, L15709 10.1029/2007GL029508 (2007).
46. E. T. Brown, T. C. Johnson, C. A. Scholz, A. S. Cohen, J. W. King, *Geophys. Res. Lett.* **34**, L20702 10.1029/2007GL031240 (2007).
47. Y. J. Wang *et al.*, *Science* **294**, 2345 (2001).
48. L. C. Peterson, G. H. Haug, K. A. Hughen, U. Rohl, *Science* **290**, 1947 (2000).
49. X. Wang *et al.*, *Nature* **432**, 740 (2004).
50. C. Placzek, J. Quade, P. J. Patchett, *Geol. Soc. Am. Bull.* **118**, 515 (2006).
51. J. C. H. Chiang, C. M. Bitz, *Clim. Dyn.* **25**, 477 (2005).
52. K. Dahl, A. Broccoli, R. Stouffer, *Clim. Dyn.* **24**, 325 (2005).
53. R. Zhang, T. L. Delworth, *J. Clim.* **18**, 1853 (2005).
54. A. Brauer, G. H. Haug, P. Dulski, D. M. Sigman, J. F. W. Negendank, *Nat. Geosci.* **1**, 520 (2008).
55. L. Benson, M. Kashgarian, M. Rubin, *Palaeogeogr. Palaeoclimatol. Palaeoecol.* **117**, 1 (1995).
56. A. Timmermann *et al.*, *J. Clim.* **20**, 4899 (2007).
57. R. Hallberg, A. Gnanadesikan, *J. Phys. Oceanogr.* **36**, 2232 (2006).
58. T. Blunier, E. J. Brook, *Science* **291**, 109 (2001).
59. A. Govin *et al.*, *Paleoceanography* **24**, PA1202 10.1029/2008PA001603 (2009).
60. D. W. J. Thompson, S. Solomon, *Science* **296**, 895 (2002).
61. G. J. Marshall, *J. Clim.* **16**, 4134 (2003).
62. G. Chen, I. M. Held, *Geophys. Res. Lett.* **34**, L21805 10.1029/2007GL031200 (2007).
63. C. Le Quéré *et al.*, *Science* **316**, 1735 (2007).
64. K. Zickfeld, J. C. Fyfe, M. Eby, A. J. Weaver, *Science* **319**, 570b (2008).
65. R. M. Law, R. J. Matear, R. J. Francey, *Science* **319**, 570a (2008).
66. A. H. Orsi, T. Whitworth, N. Worth, *Deep-Sea Res.* **42**, 641 (1995).
67. N. J. Shackleton, M. A. Hall, J. Line, C. Shuxi, *Nature* **306**, 319 (1983).
68. EPICA Community Members, *Nature* **429**, 623 (2004).
69. E. Monnin *et al.*, *Earth Planet. Sci. Lett.* **224**, 45 (2004).
70. P. J. Reimer *et al.*, *Radiocarbon* **46**, 1029 (2004).
71. H. Rashid, R. Hesse, D. J. W. Piper, *Earth Planet. Sci. Lett.* **205**, 281 (2003).

72. Work described in this paper was funded by a grants/cooperative agreement from the National Oceanic and Atmospheric Administration, by the National Science Foundation, and by the Norwegian Research Council and the Norwegian Polar Institute as part of VISTA project 6535. The views expressed herein are those of the authors and do not necessarily reflect the views of NOAA or any of its sub-agencies. Comments on earlier drafts of the manuscript by J. R. Toggweiler, L. K. Armand, and M.-E. Carr led to substantial improvements. W. S. Broecker brought to our attention the importance of paleo lake level records. Discussions with P. de Menocal, J. McManus, and D. Martinson helped clarify our thinking about processes discussed in this paper. Comments from two anonymous reviewers improved the manuscript. Samples from TN057 cores were provided by the repository at Lamont-Doherty Earth Observatory; samples from E27-23 were provided by the Antarctic Marine Geology Research Facility at Florida State University.

Supporting Online Material

www.sciencemag.org/cgi/content/full/323/5920/1443/DC1
SOM Text
Figs. S1 to S4
Tables S1 to S4
References

20 October 2008; accepted 9 February 2009
10.1126/science.1167441

The Dynamic Control of Kiss-And-Run and Vesicular Reuse Probed with Single Nanoparticles

Qi Zhang, Yulong Li, Richard W. Tsien*

Vesicular secretion of neurotransmitter is essential for neuronal communication. Kiss-and-run is a mode of membrane fusion and retrieval without the full collapse of the vesicle into the plasma membrane and de novo regeneration. The importance of kiss-and-run during efficient neurotransmission has remained in doubt. We developed an approach for loading individual synaptic vesicles with single quantum dots. Their size and pH-dependent photoluminescence change allowed us to distinguish kiss-and-run from full-collapse fusion and to track single vesicles through multiple rounds of kiss-and-run and reuse, without perturbing vesicle cycling. Kiss-and-run dominated at the beginning of stimulus trains, reflecting the preference of vesicles with high release probability. Its incidence was increased by rapid firing, a response appropriate to shape the kinetics of neurotransmission during a wide range of firing patterns.

As a keystone of neuronal communication, the exocytosis and endocytosis of synaptic vesicles may take different forms (*1*). In full-collapse fusion (FCF), vesicles flatten completely into the plasma membrane, lose their identity, and must be replaced eventually by newly generated vesicles (*2*). In contrast, transient fusion and retrieval, often called "kiss-and-run" (K&R), would preserve a limited supply of releasable vesicles for reuse (*3*). Although nonclassical modes akin to K&R have been demonstrated in non-neuronal cells (*4*–*8*) and in a specialized calyceal synapse (*9*), it remains uncertain whether K&R is appreciable in small nerve terminals typical of the mammalian brain, which rely on only a few dozen releasable vesicles (*8*, *10*). Vesicle recycling in these terminals has been studied by optical reporters such as styryl dyes or synaptopHluorin (synaptophysin fused with pH-sensitive green fluorescent protein) (*11*–*15*). However, the limited signal-to-noise (S/N) ratio of such probes has left uncertainty about the functional impact of K&R.

Quantum dots have been widely used for applications requiring high S/N ratios (*16*–*18*). Those with peak emission at 605 nm and a diameter of ~15 nm (Qdots hereafter; fig. S1A) provided suitable artificial cargo: small enough to fit into the vesicular lumen (~24 nm), yet large enough to be rejected by putative K&R fusion pores (1 to 5 nm) (*9*, *19*). Furthermore, the pH dependence of Qdot emission (*17*) would allow reporting of exocytotic events, similar to pHluorin-based indicators (*20*, *21*).

Imaging single Qdot-loaded vesicles. Sparse Qdot loading was accomplished by mildly stimulating neurons. Functional synapses in the Qdot images were identified by subsequent FM4-64 staining (Fig. 1A). At many FM4-64–positive synapses, the Qdot signal was close to background ($P > 0.10$, t test), indicating no Qdot uptake (Fig. 1A). The remaining synapses (~42%) showed higher intensities distributed in two evenly spaced peaks (Fig. 1A). The interpeak spacing matched the unitary Qdot signal determined by blinking, a spontaneous intermittency of photoluminescence (*22*) ($P > 0.25$, t test). This calibration (*23*, *24*) confirmed that peak 1 corresponded to uptake of a single Qdot per synapse.

Qdot photoluminescence was pH-dependent: It increased by ~15% when pH was raised from 5.48 (intravesicular) to 7.34 (extracellular) (Fig. 1B). Indeed, photoluminescence of single Qdots in pH 7.34 agarose gel [72.1 ± 2.1 arbitrary units (a.u.), $n = 371$] exceeded that in nerve terminals by ~15% ($P < 0.01$, t test), a difference reversibly nullified by perfusion with pH 5.48 solution (fig. S2C). These data suggested that synapse-loaded Qdots were harbored at pH ~5.5, presumably within synaptic vesicles, as seen directly in electron microscopy images (*25*).

The pH dependence predicted distinct patterns of Qdot photoluminescence upon K&R and FCF (Fig. 1B): K&R would allow protons but not the Qdot to escape, causing transient deacidification and Qdot brightening. FCF would appear as similar Qdot brightening followed by loss of signal as the Qdot departs.

Qdots unambiguously identify FCF and K&R. Qdot-loaded boutons did exhibit different patterns of photoluminescence upon stimulation (0.1 Hz, 2 min; Fig. 1C): (i) baseline noise, (ii) a transient positive deflection (uptick), (iii) an uptick followed immediately by a negative step (downstep), and (iv) patterns ii and iii in sequence. The uptick level showed as a distinct peak ~15% above baseline, distinct from baseline noise (Fig. 1D). Amplitudes of the upticks with or without downsteps were the same (~9.9 a.u., fig. S3A). Invariably, downsteps followed an uptick, were irreversible (236/236 events, fig. S3B), and were identical in amplitude to that of single Qdots ($P > 0.25$, t test), consistent with the disappearance of Qdots after FCF. With or without downsteps, the great majority of upticks were stimulus-locked

Department of Molecular and Cellular Physiology, Stanford University, Stanford, CA 94305, USA.

*To whom correspondence should be addressed. E-mail: rwtsien@stanford.edu

(Fig. 1C, Fig. 2, and Fig. 3B), with latency briefer than the image acquisition interval (fig. S3, C and D). Some traces (8.6%) included events that were not clearly stimulus-locked (fig. S3C), presumably reflecting spontaneous exocytosis.

The upticks were probed by blocking vesicular H^+ transport with bafilomycin A1 (Baf). Without Baf, all nonblank records could be classified as K&R alone, FCF alone, or K&R + FCF in succession (Fig. 1C and Fig. 2). With acute exposure to Baf, which spares the pre-exocytotic pH gradient but prevents postexocytotic reacidification (*25*), isolated upticks were replaced by persistent increases (upsteps) of the same amplitude (10.47 ± 1.14 a.u., n = 49). This was expected if Qdots remained in post-K&R vesicles that failed to reacidify. After an upstep, subsequent uptick-downsteps were replaced by simple downsteps, 73.6 ± 3.4 a.u. (n = 157), 115% of the basal Qdot signal. After 1 hour of Baf incubation, which abolishes both the existing pH gradient and vesicular reacidification (*26*), prestimulation photoluminescence rose to ~115% of control, and no further increase was ever observed upon stimulation; all downsteps proceeded without a prior uptick. The amplitudes of upticks, upsteps, and downsteps showed expected interrelationships (fig. S4). Note that upsteps were never observed in the absence of Baf, contrary to expectations if Qdots externalized by FCF had clung on long enough to be recaptured by conventional endocytosis [time constant, τ, estimated at 14, 17, and 48 s, respectively, in (*13*, *14*, *27*)]. Instead, the upticks can be attributed to vesicular retention of the Qdot and reacidification upon closure of a fusion pore.

This interpretation was tested further by increasing external pH buffering with 50 mM Tris

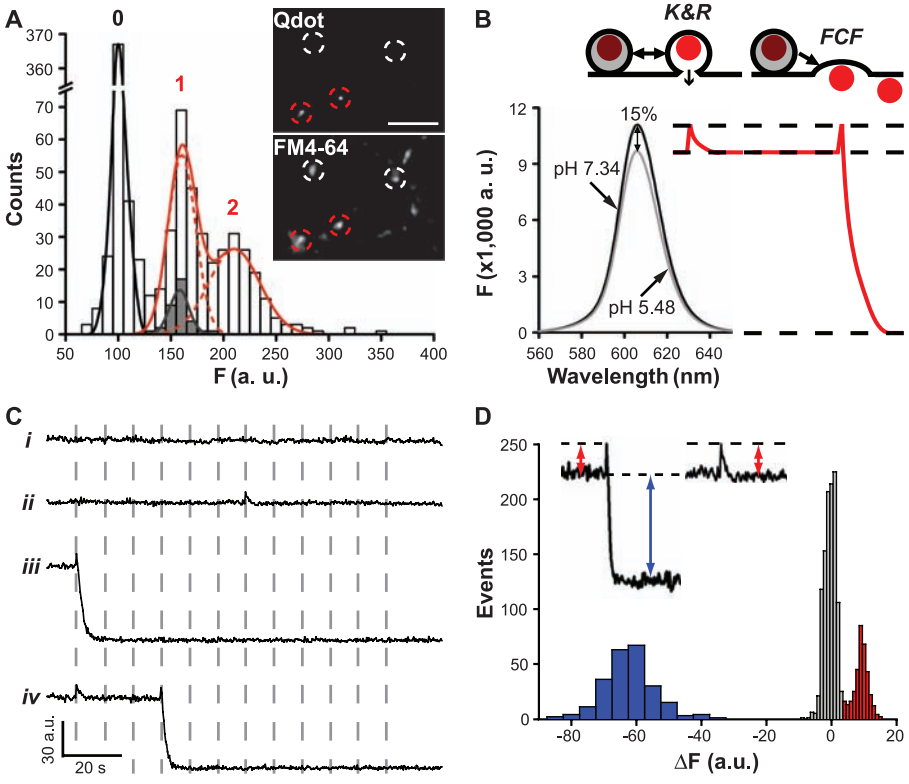

Fig. 1. Single Qdots loaded into synaptic boutons exhibit distinct patterns of photoluminescence change. (**A**) Neurons stimulated (10 Hz, 1 s) with 400 nM Qdots present, then thoroughly washed. The distribution of photoluminescent intensity was measured at FM4-64–defined regions of interest. Best fit was obtained with three evenly spaced Gaussians (black line and red dashed lines labeled 0, 1, and 2; red line indicates the summation of Gaussians 1 and 2), 63.9 a.u. apart. Spacing agrees with amplitude of blinking events (gray bars with the black line indicating a Gaussian fitting; mean 61.3 ± 4.5 a.u.) (P > 0.25, t test). Inset: Circles mark functional boutons identified by FM4-64 staining, with (red) or without (white) single Qdot loading. Scale bar, 3 μm. (**B**) pH-dependent Qdot photoluminescence. Cartoons show hypothetical Qdot signals arising from pH dependence. (**C**) Photoluminescence traces recorded during 0.1-Hz field stimulation for 2 min (dashed lines). (**D**) Upon stimulation, changes in Qdot signal (ΔF) could be classified as noise (gray bars, centered at 0 a.u.) or a clear positive deflection (red bars, centered at ~9 a.u., >2.5 SD of noise), ~15% of size of subsequent negative deflections (blue bars, centered at ~ −63 a.u.). Insets indicate measurements leading to the corresponding histograms.

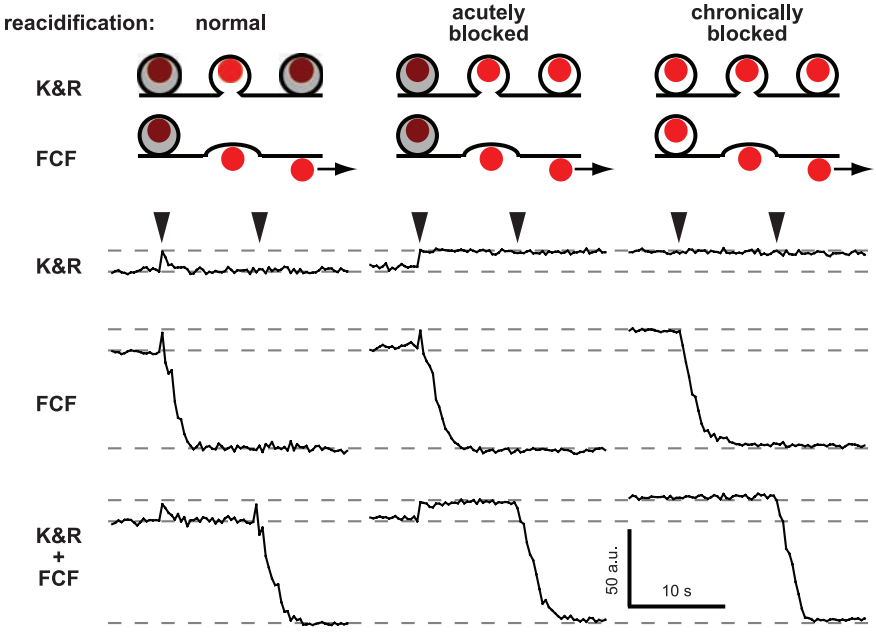

Fig. 2. Upward transients in Qdot signal report pH changes within the vesicle lumen. Cartoons show hypothesized effect of acute or chronic block of vesicular H^+–adenosine triphosphatase with bafilomycin A1 (Baf). Without Baf (normal), Qdot photoluminescence is diminished (maroon) by acidic luminal pH (gray). Deacidification upon vesicle fusion removes this quenching and Qdot brightens (red). Acute application of Baf (acutely blocked) prevents reacidification after vesicle retrieval; chronic Baf (chronically blocked) removes all pH gradients. Experimental traces illustrate typical photoluminescence patterns under three conditions. Patterns are classified as K&R, FCF, or K&R + FCF (labeled rows) according to analysis of collected data (fig. S4).

instead of 10 mM HEPES (pH_o always 7.3). If Tris entered the vesicle and remained sequestered along with the Qdot, luminal reacidification should be slowed (*12*). Indeed, the uptick decay was longer ($P < 0.01$, *t* test; fig. S5A). In contrast, the time course of uptick-downsteps remained unchanged with Tris (fig. S5B), as expected for externalized Qdots.

Tracking the motion of single Qdots during and after fusion (movie S1) buttressed our interpretation of the two kinds of Qdot signals (supporting online text). Downsteps were always associated with the Qdot moving out of synapses (fig. S6); the diffusion coefficient, $D = 1.7 \pm 0.1\ \mu m^2/s$, resembled that of Qdots tethered to membrane proteins (*28*). In contrast, in instances of uptick alone, Qdots remained close to their position at the moment of fusion (displacement 50 ± 6 nm, $n = 43$), consistent with the idea of K&R as "retrieval on the spot" (*29*). Was the Qdot-reported K&R inadvertently promoted by Qdot adherence? Previous findings with FM4-64 coloaded with Qdots argued against this idea (*25*). For further verification, we monitored vesicle cycling with the use of pHluorin-tagged vesicular glutamate transporter 1 (*30*) but found no difference in vesicle dynamics before, during, or after maximal loading with Qdots (fig. S7).

Timing and prevalence of K&R and FCF. The all-or-none nature of Qdot uptake allowed us to track a single vesicle in the total recycling pool (TRP) until its final FCF. Labeling of individual vesicles in the TRP was obtained with strong stimulation (10 Hz, 2 min) at low Qdot concentration (4 nM). Among 793 vesicles in single Qdot–loaded boutons, 302 exhibited fusion and are represented as raster lines (Fig. 3A); the others showed no fusion with field stimulation but only with later high K^+ challenges. Of the 302 vesicles, 292 fused upon field stimulation; of these, 13 showed one K&R, 58 showed one K&R followed by FCF, 1 showed two K&R events, and 220 showed FCF only. Thus, K&R occurred in ~25% of all vesicles and accounted for 21% of all fusion events over the field stimulation.

Intriguingly, the prevalence of K&R and FCF was dependent on stimulus number. K&R events were predominant initially (63.4 ± 9.9% at first stimulus) but became less prevalent as stimulation continued (Fig. 3C), falling to <10% later in the train (Fig. 3E). Because Qdots can report FCF after K&R but not vice versa, we examined first-fusion events specifically, and found the same trend.

K&R is favored by RRP vesicles. What is the basis of the decaying K&R ratio? One possibility is that vesicles with higher release probability per vesicle ($P_{r/v}$), namely readily releasable pool (RRP) vesicles, prefer K&R (*31*, *32*). Alternatively, the shift in fusion modes might arise from a cumulative effect of electrical activity, independent of $P_{r/v}$. To test these ideas, we prefaced field stimulation with a hypertonic challenge to selectively mobilize RRP vesicles without electrical activity or Ca^{2+} elevation (*33*). Rapid application of Tyrode's solution + 500 mM sucrose for 10 s caused vesicular turnover, reflected by upticks and uptick-downsteps whose peak-aligned averages were virtually identical to the corresponding responses to electrical stimulation. The two types of events were similarly timed [$P > 0.1$, Kolmogorov-Smirnov (K-S) test] and clustered between 1 and 7 s after the hypertonic challenge started. The hypertonic challenge elicited more K&R than FCF (Fig. 3E), yielding a K&R ratio (0.63 ± 0.05) similar to that found with the first field stimulus. During the subsequent electrical stimulation, the numbers of K&R and FCF events held steady, then fell in parallel as Qdot-labeled vesicles were depleted (Fig. 3E). Consequently, the K&R ratio stayed at ~15% during the whole stimulus train (Fig. 3F). Thus, RRP-resident vesicles displayed a strong propensity for K&R, but once-fused RRP vesicles and vesicles freshly recruited from the reserve pool were less favorably disposed to K&R, thus accounting for the observed drop in the K&R ratio.

K&R increases upon rapid stimulation. Hippocampal neurons often fire in bursts with intraburst frequencies far greater than 0.1 Hz. A key question is whether the balance between modes of fusion tilts when neurotransmission intensifies. Accordingly, after single Qdots had been loaded into the TRP, we applied 10-Hz field stimulation for 2 min. The fusion rate clearly increased (Fig. 4A). Qdot-loaded vesicles were sorted according to their behavior during the stimulation (Fig. 4B). Again, the prevalence of K&R started high but fell with continual stimulation (Fig. 4C). The initial contribution of K&R was significantly greater at 10 Hz (~88%) than at 0.1 Hz (~62%; $P < 0.05$, *t* test); likewise for the later steady level of K&R prevalence (~30% versus 10%; $P < 0.05$, *t* test). Among Qdot-labeled vesicles responding to electrical stimulation, 68% supported one or more K&R events, considerably more than with 0.1-Hz stimulation, and this effect likely extended beyond the RRP (<30% of vesicles) (*11*, *32*, *33*). At 10 Hz, individual vesicles supported as many as three rounds of K&R before a final FCF (Fig. 4A). Various combinations of fusion and retrieval events were observed (Fig. 4B).

To clarify the increase in reuse, we sorted Qdot-loaded vesicles according to overall performance and plotted the respective latencies to first fusion. Of the vesicles undergoing FCF alone, ~84% fused

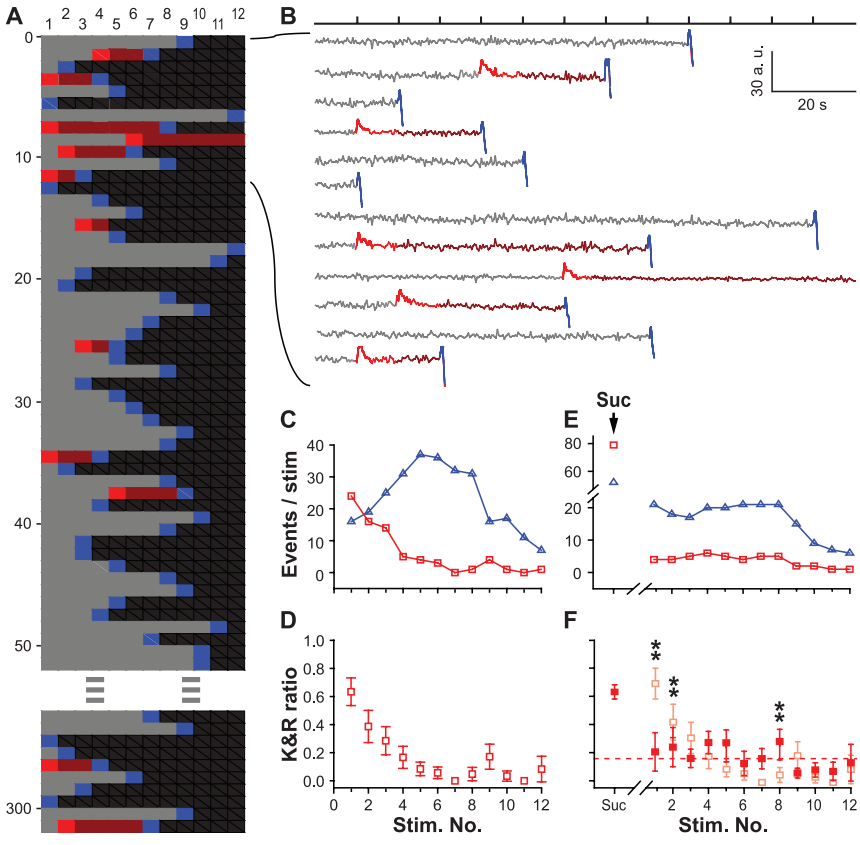

Fig. 3. Prevalence of K&R changes over the course of stimulation as RRP vesicles are depleted. (**A**) Raster representation of traces ($n = 302$) from single Qdot-loaded vesicles that responded to 0.1-Hz field stimulation for 2 min. For each stimulus and subsequent interval, Qdot signals registered as nonresponse (gray), K&R (red), nonresponse after K&R (maroon), FCF (blue), or Qdot no longer present in region of interest (black). Pooled traces from $N = 8$ cover slips, three separate cultures. (**B**) Traces corresponding to the first 12 rasters in (A). Photoluminescence changes are color-coded for each stimulus and ensuing interval as in (A). (**C**) Numbers of K&R (red squares) and FCF events (blue triangles), plotted for every stimulus. (**D**) K&R ratio for every stimulus ($N = 8$). Vertical bars are ±SEM. (**E**) Numbers of K&R (red squares) and FCF events (blue triangles), plotted for prestimulation hypertonic challenge (suc) and for each field stimulus. (**F**) Corresponding K&R ratio (solid red squares), compared with control [faded red squares, copied from (D)] (**$P < 0.01$, χ^2 test).

with a delay of >30 s, late enough to ensure that they originated from the reserve pool rather than the RRP (*11*, *32*). In contrast, all vesicles generating three K&R events first fused within <30 s. Overall, the earlier the first fusion of a vesicle (higher $P_{r/v}$), the more K&R it supported (Fig. 4D). This was not simply due to a longer time span from stimulation onset to final FCF, because this span was independent of the number of K&R events (fig. S8). Instead, residence in the RRP (and high $P_{r/v}$) favors K&R, in agreement with findings with hypertonic challenges (Fig. 3, E and F).

How soon after K&R can a vesicle be reused under rapid stimulation? We focused on cases wherein two consecutive K&R events were followed by FCF, to obtain a balanced comparison between K-K intervals (i.e., elapsed time between two consecutive K&R events) and K-F intervals (i.e., elapsed time between K&R and ensuing FCF). K-K intervals (Fig. 4E) were briefer (shortest, 2.67 s; median, 5.67 s; average, 10.26 ± 2.04 s) and faster than the classic exocytosis-endocytosis cycle in hippocampal terminals (*8*). In contrast, the K-F interval (Fig. 4E) was longer than the K-K interval by a factor of ~3 (median, 22.3 s; average, 26.8 ± 3.6 s). However, the K-F interval was faster than the latency to FCF only by a factor of 3 (~60 s); vesicles undergoing reuse by FCF after K&R still enjoyed a big kinetic advantage over unused vesicles destined for FCF.

Rapid reacidification and activity-dependent fusion pore open time. For functional advantage, speedy reuse of vesicles must be complemented by prompt fusion pore closure and fast reacidification, so as to allow vesicular refilling with neurotransmitter (*34*) and avoid "shooting blanks." Using 30-Hz imaging, we found that once the Qdot signal increased upon stimulation (single pulse; intertrial interval ~20 s), it remained at the highest level for a variable time before returning to baseline (Fig. 5A, inset). Such a plateau was expected while the fusion pore remained open. Indeed, experimental traces were better fitted with a plateau preceding a single-exponential decay than with an exponential alone (Fig. 5A). The median plateau duration was 0.367 s (average 0.527 ± 0.085 s, $n = 43$) and the median time constant of decay was 0.69 s (average 0.95 ± 0.18 s, $n = 43$). To verify the separation of plateau and decay phases, we again applied 50 mM Tris (Fig. 5, B and C). The Qdot signal showed the same amplitude and plateau duration as with HEPES (Fig. 5F; both $P > 0.5$, K-S test) while the decay was slowed (Fig. 5F; $P < 0.01$, K-S test), as also seen with low-frequency imaging (fig. S5A). The buffer insensitivity of the plateau amplitude and duration confirmed that the plateau represented the period preceding vesicle reacidification.

Because H^+ transport is the likely rate-limiting step for transmitter refilling (*1*, *34*), full reestablishment of ΔpH suggests that transmitter refilling was also nearly complete. Our direct measurements yield a vesicle reacidification rate faster than most previous estimates (*13*, *14*), with one exception (*12*). To probe whether the fusion pore open time and the vesicle reacidification rate are subject to change, we applied 10-Hz stimulation for 5 s. The plateau duration became longer (Fig. 5, D and E), increasing from ~0.5 s to 1.05 ± 0.18 s ($n = 46$), but both plateau amplitude and recovery time constant of decay, τ_{decay}, remained unaltered (Fig. 5F). Thus, reacidification proceeded rapidly at 10 Hz ($\tau_{decay} = 0.99 \pm 0.12$ s, $n = 46$), just as it did at low frequency. The frequency-dependent lengthening of plateau duration developed gradually during the 10-s stimulation train ($P < 0.01$, Pearson correlation test), indicating again that fusion pore gating was under physiological control.

Discussion. Using Qdots, we developed a method to distinguish multiple fusion modes with sharply different optical signals and single-event resolution, which enabled us to clarify the uncertainty about K&R at small nerve terminals of the central nervous system (*11*–*14*, *26*, *35*). As indivisible nanoparticles, Qdots could label individual vesicles in either the RRP or the reserve pool, which allowed us to monitor them without loss of signal continuity or amplitude through multiple rounds of reuse. In future studies, Qdots of different sizes and colors could be used to manipulate the vesicular volume available for neurotransmitter or to track different vesicles. Furthermore, Qdots might be engineered to give a larger pH-dependent signal and to permanently attach to the presynaptic membrane, enabling long-term tracking of presynaptic activity in situ.

Using Qdots, we could characterize the rapid reuse of vesicles. K&R gradually gave way to FCF as the dominant fusion mode during a stimulus train, contrary to the simple assumption of a fixed ratio (*26*). Consequently, K&R and FCF can each be predominant under different conditions. K&R appears most prominent under high-activity demand. FCF outweighs K&R under steady-state stimulation at low rates—that is, under conditions typical of studies in which K&R has been difficult to detect (*13*, *14*, *35*).

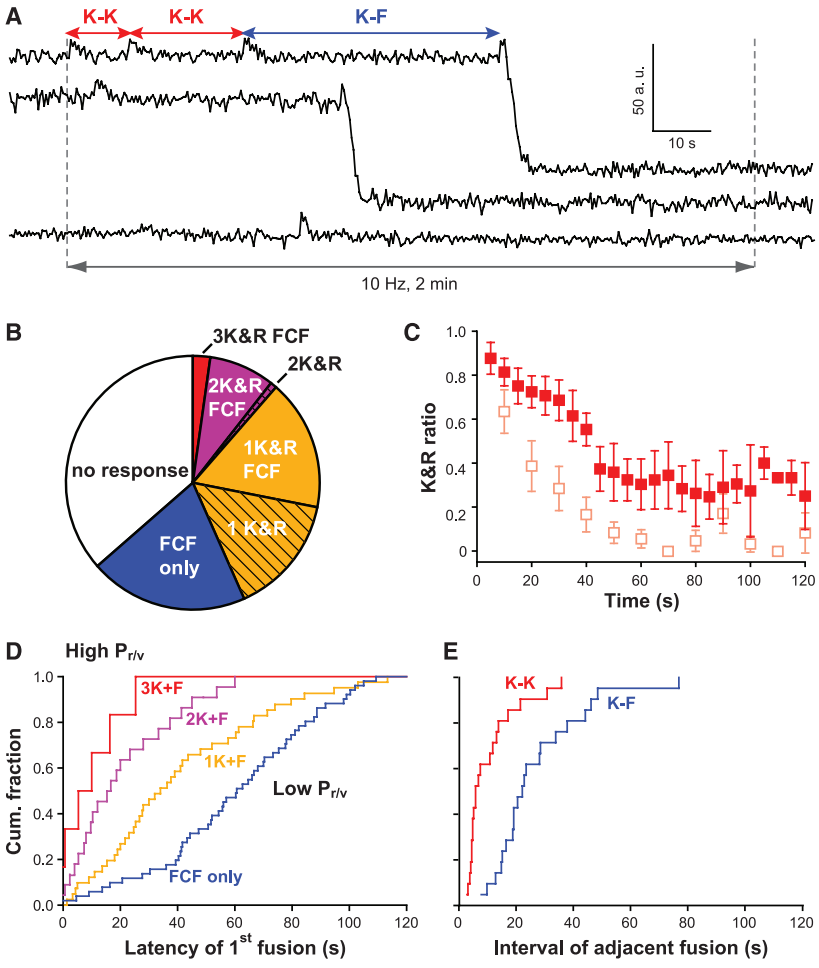

Fig. 4. Up-modulation of K&R prevalence with intense stimulation. (**A**) Sample traces from Qdot-loaded vesicles. (**B**) Categorization of vesicles with different fusion behaviors. (**C**) The K&R ratio during 10-Hz stimulation for 2 min (analyzed with 5-s time bins to improve S/N) was significantly higher than that during 0.1-Hz stimulation (faded symbols, data from Fig. 3D). (**D**) Latency of first fusion in the different categories [same color coding as (B)]. Each plot normalized by the number of vesicles in that category. The higher its $P_{r/v}$, the more K&R events a vesicle could support ($P_{r/v}$ = 0.051, 0.023, 0.010, and 0.001, respectively, for 3K + F, 2K + F, K + F, and FCF only). (**E**) The interval between two consecutive K&R events (K-K, red) was significantly shorter than that between K&R and a subsequent FCF of the same vesicle (K-F, blue) ($P < 0.01$, K-S test).

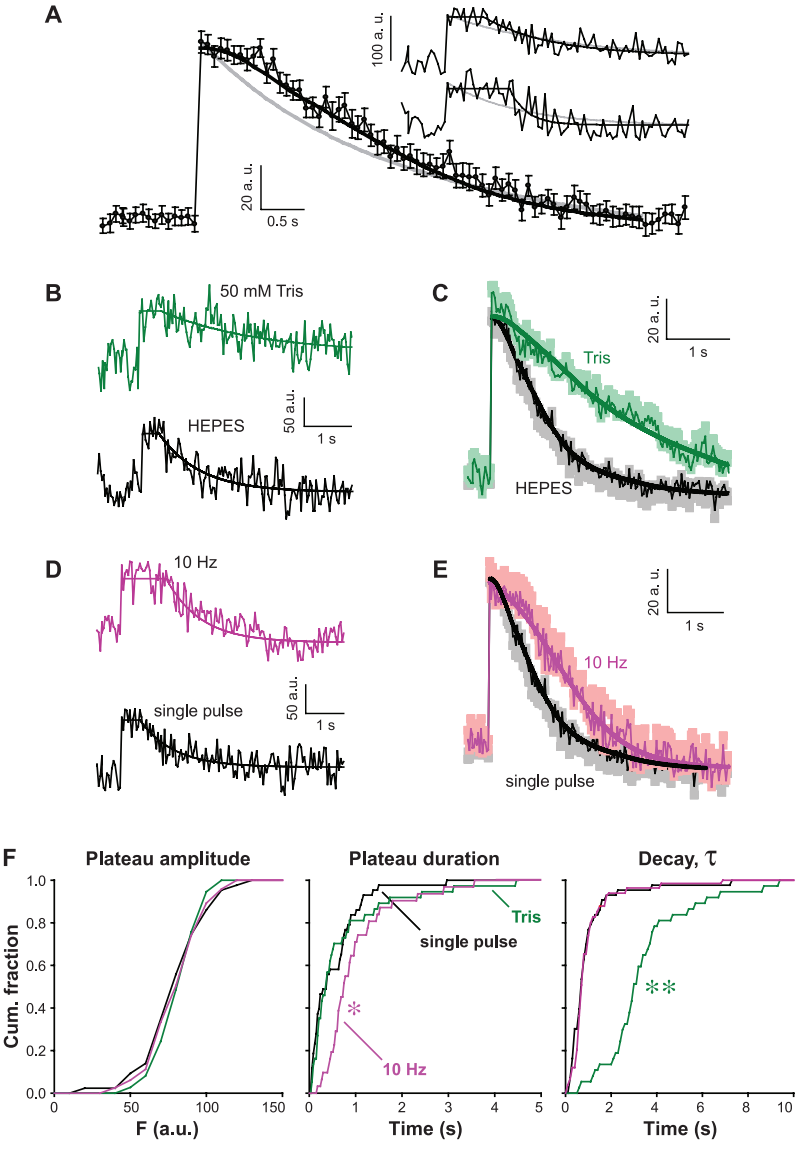

Fig. 5. High-speed imaging of Qdots reveals adjustable fusion pore open time but constant vesicle reacidification rate with different levels of activity. (**A**) Comparison of pooled data exemplified by insets (black symbols with error bars indicating SEM, $n = 43$) and averages of the two kinds of fits (gray and black). Insets: Samples taken in normal Tyrode's solution with single shocks; interstimulus interval, >20 s. Two types of fits were overlaid: a single-exponential decay (gray) and a plateau followed by an exponential (black), the latter fitting significantly better even after statistical penalization for the extra parameter (Akaike information criterion score, –60.5; $P < 0.001$). (**B**) Samples in 50 mM Tris (green) and in 10 mM HEPES (black). (**C**) Corresponding pooled data in Tris ($n = 37$) and in HEPES [same as (A)]. (**D**) Samples (normal Tyrode's solution) with 10-Hz (pink) and single-pulse stimulation (black). Smooth lines are corresponding fits as above. (**E**) Pooled data taken with 10-Hz ($n = 46$) and single-pulse stimulation [same as (A)]. (**F**) Cumulative distributions of fit parameters. Plateau amplitude: distributions were not different (all $P > 0.1$, K-S test); plateau duration: only distribution for 10-Hz stimulation was longer (*$P < 0.01$, K-S test); τ_{decay}: only distribution for 50 mM Tris was slower (**$P < 0.001$, K-S test).

The duration of fusion pore opening (0.5 to 1 s) was in good agreement with the capacitance measurements in the calyx of Held (*9*) and chromaffin cells (*36*). A subsecond opening would easily allow complete emptying of small neurotransmitters. Further study is needed to determine whether flickering or gradual widening of the fusion pore (*37*, *38*) allows gradual release of neurotransmitter and postsynaptic receptor desensitization at excitatory synapses.

K&R confers multiple functional advantages. Some RRP vesicles could fuse up to four times, allowing more efficient recycling, particularly with the intermittent patterns of burst firing found for hippocampal neurons in vivo. The rate of vesicle reuse we recorded was much faster than could be previously estimated (*11*)—a kinetic advantage if reuse of the same vesicle is an alternative to readying a fresh vesicle at the same release site. Nonetheless, the shortest interval between successive fusion events still left enough time for nearly complete reacidification (and, by inference, replenishment with neurotransmitter), consistent with preservation of quantal size even at high firing rates (*39*). On the other hand, persistent occupancy of release sites by a K&R vesicle awaiting reuse might also contribute to "release site inactivation" and falling $P_{r/v}$ during sustained firing.

With regard to synaptic variability, the repeated reuse of a small population of vesicles in successive bursts (*11*) would reduce variations in neurotransmitter content arising from differences in vesicle volume or in luminal transmitter concentration (*34*). Reuse of the same release site would also lower "release location–dependent variability" (*40*). In both ways, reuse would improve the fidelity of information transfer during neurotransmission.

References and Notes

1. T. C. Südhof, *Annu. Rev. Neurosci.* **27**, 509 (2004).
2. J. E. Heuser, T. S. Reese, *J. Cell Biol.* **57**, 315 (1973).
3. R. Fesce, F. Grohovaz, F. Valtorta, J. Meldolesi, *Trends Cell Biol.* **4**, 1 (1994).
4. G. Alvarez de Toledo, R. Fernandez-Chacon, J. M. Fernandez, *Nature* **363**, 554 (1993).
5. C. R. Artalejo, J. R. Henley, M. A. McNiven, H. C. Palfrey, *Proc. Natl. Acad. Sci. U.S.A.* **92**, 8328 (1995).
6. J. W. Taraska, D. Perrais, M. Ohara-Imaizumi, S. Nagamatsu, W. Almers, *Proc. Natl. Acad. Sci. U.S.A.* **100**, 2070 (2003).
7. T. Fulop, S. Radabaugh, C. Smith, *J. Neurosci.* **25**, 7324 (2005).
8. S. M. Smith, R. Renden, H. von Gersdorff, *Trends Neurosci.* **31**, 559 (2008).
9. L. He, X. S. Wu, R. Mohan, L. G. Wu, *Nature* **444**, 102 (2006).
10. S. An, D. Zenisek, *Curr. Opin. Neurobiol.* **14**, 522 (2004).
11. A. M. Aravanis, J. L. Pyle, R. W. Tsien, *Nature* **423**, 643 (2003).
12. S. P. Gandhi, C. F. Stevens, *Nature* **423**, 607 (2003).
13. B. Granseth, B. Odermatt, S. J. Royle, L. Lagnado, *Neuron* **51**, 773 (2006).
14. J. Balaji, T. A. Ryan, *Proc. Natl. Acad. Sci. U.S.A.* **104**, 20576 (2007).
15. X. Chen, S. Barg, W. Almers, *J. Neurosci.* **28**, 1894 (2008).
16. A. P. Alivisatos, W. Gu, C. Larabell, *Annu. Rev. Biomed. Eng.* **7**, 55 (2005).
17. X. Gao, W. C. Chan, S. Nie, *J. Biomed. Opt.* **7**, 532 (2002).
18. M. Heine *et al.*, *Science* **320**, 201 (2008).
19. M. B. Jackson, E. R. Chapman, *Annu. Rev. Biophys. Biomol. Struct.* **35**, 135 (2006).
20. G. Miesenböck, D. A. De Angelis, J. E. Rothman, *Nature* **394**, 192 (1998).
21. S. Sankaranarayanan, T. A. Ryan, *Nat. Cell Biol.* **2**, 197 (2000).
22. M. Nirmal *et al.*, *Nature* **383**, 802 (1996).
23. M. Howarth, K. Takao, Y. Hayashi, A. Y. Ting, *Proc. Natl. Acad. Sci. U.S.A.* **102**, 7583 (2005).
24. B. Cui *et al.*, *Proc. Natl. Acad. Sci. U.S.A.* **104**, 13666 (2007).
25. Q. Zhang, Y. Q. Cao, R. W. Tsien, *Proc. Natl. Acad. Sci. U.S.A.* **104**, 17843 (2007).
26. N. C. Harata, S. Choi, J. L. Pyle, A. M. Aravanis, R. W. Tsien, *Neuron* **49**, 243 (2006).
27. V. J. Mueller, M. Wienisch, R. B. Nehring, J. Klingauf, *J. Neurosci.* **24**, 2004 (2004).
28. M. Dahan *et al.*, *Science* **302**, 442 (2003).
29. F. Valtorta, J. Meldolesi, R. Fesce, *Trends Cell Biol.* **11**, 324 (2001).
30. S. M. Voglmaier *et al.*, *Neuron* **51**, 71 (2006).
31. C. F. Stevens, J. H. Williams, *Proc. Natl. Acad. Sci. U.S.A.* **97**, 12828 (2000).
32. J. L. Pyle, E. T. Kavalali, E. S. Piedras-Renteria, R. W. Tsien, *Neuron* **28**, 221 (2000).
33. C. Rosenmund, C. F. Stevens, *Neuron* **16**, 1197 (1996).
34. R. H. Edwards, *Neuron* **55**, 835 (2007).
35. T. Fernandez-Alfonso, T. A. Ryan, *Neuron* **41**, 943 (2004).
36. S. A. Chan, C. Smith, *J. Physiol.* **537**, 871 (2001).
37. R. G. Staal, E. V. Mosharov, D. Sulzer, *Nat. Neurosci.* **7**, 341 (2004).

38. S. Choi, J. Klingauf, R. W. Tsien, *Philos. Trans. R. Soc. London Ser. B* **358**, 695 (2003).
39. Q. Zhou, C. C. Petersen, R. A. Nicoll, *J. Physiol.* **525**, 195 (2000).
40. K. M. Franks, C. F. Stevens, T. J. Sejnowski, *J. Neurosci.* **23**, 3186 (2003).
41. We thank N. C. Harata for help with high-frequency imaging and data analysis, R. J. Reimer and members of the Tsien lab for comments, J. W. Mulholland and J. J. Perrino for help with imaging, and X. Gao and M. Bruchez for consultation on quantum dots. Supported by grants from the Grass Foundation (Q.Z.), the National Institute of Mental Health, and the Burnett Family Fund (R.W.T.).

Supporting Online Material
www.sciencemag.org/cgi/content/full/1167373/DC1
Materials and Methods
Figs. S1 to S9
Movie S1
References

20 October 2008; accepted 27 January 2009
Published online 12 February 2009;
10.1126/science.1167373
Include this information when citing this paper.

Explosive Percolation in Random Networks

Dimitris Achlioptas,[1] Raissa M. D'Souza,[2,3]* Joel Spencer[4]

Networks in which the formation of connections is governed by a random process often undergo a percolation transition, wherein around a critical point, the addition of a small number of connections causes a sizable fraction of the network to suddenly become linked together. Typically such transitions are continuous, so that the percentage of the network linked together tends to zero right above the transition point. Whether percolation transitions could be discontinuous has been an open question. Here, we show that incorporating a limited amount of choice in the classic Erdös-Rényi network formation model causes its percolation transition to become discontinuous.

A large system is said to undergo a phase transition when one or more of its properties change abruptly after a slight change in a controlling variable. Besides water turning into ice or steam, other prototypical phase transitions are the spontaneous emergence of magnetization and superconductivity in metals, the epidemic spread of disease, and the dramatic change in connectivity of networks and lattices known as percolation. Perhaps the most fundamental characteristic of a phase transition is its order, i.e., whether the macroscopic quantity it affects changes continuously or discontinuously at the transition. Continuous (smooth) transitions are called second-order and include many magnetization phenomena, whereas discontinuous (abrupt) transitions are called first-order, a familiar example being the discontinuous drop in entropy when liquid water turns into solid ice at 0°C.

We consider percolation phase transitions in models of random network formation. In the classic Erdös-Rényi (ER) model (*1*), we start with n isolated vertices (points) and add edges (connections) one by one, each edge formed by picking two vertices uniformly at random and connecting them (Fig. 1A). At any given moment, the (connected) component of a vertex v is the set of vertices that can be reached from v by traversing edges. Components merge under ER as if attracted by gravitation. This is because every time an edge is added, the probability two given components will be merged is proportional to the number of possible edges between them which, in turn, is equal to the product of their respective sizes (number of vertices).

One of the most studied phenomena in probability theory is the percolation transition of ER random networks, also known as the emergence of a giant component. When rn edges have been added, if $r < ½$, the largest component remains miniscule, its number of vertices C scaling as $\log n$; in contrast, if $r > ½$, there is a component of size linear in n. Specifically, $C \approx (4r - 2)n$ for r slightly greater than ½ and, thus, the fraction of vertices in the largest component undergoes a continuous phase transition at $r = ½$ (Fig. 1C). Such continuity has been considered a basic characteristic of percolation transitions, occurring in models ranging from classic percolation in the two-dimensional grid to random graph models of social networks (*2*).

Here, we show that percolation transitions in random networks can be discontinuous. We demonstrate this result for models similar to ER, thus also establishing that altering a network-formation process slightly can affect it dramatically, changing the order of its percolation transition. Concretely, we consider models that, like ER, start with n isolated vertices and add edges one by one. The difference, as illustrated in Fig. 1B, is that to add a single edge we now first pick two random edges $\{e_1,e_2\}$, rather than one, each edge picked exactly as in ER and independently of the other. Of these, with no knowledge of future edge-pairs, we are to select one and insert it in the graph and discard the other. Clearly, if we always resort to randomness for selecting among the two edges, we recover the ER model. Whether nonrandom selection rules can delay (or accelerate) percolation in such models, which have become known as Achlioptas processes, has received much attention in recent years (*3*–*6*).

[1]Department of Computer Science, University of California at Santa Cruz, Santa Cruz, CA 95064, USA. [2]Department of Mechanical and Aeronautical Engineering, University of California at Davis, Davis, CA 95616, USA. [3]Santa Fe Institute, 1399 Hyde Park Road, Santa Fe, NM 87501, USA. [4]Courant Institute of Mathematical Sciences, New York University, New York, NY 10012, USA.

*To whom correspondence should be addressed. E-mail: raissa@cse.ucdavis.edu

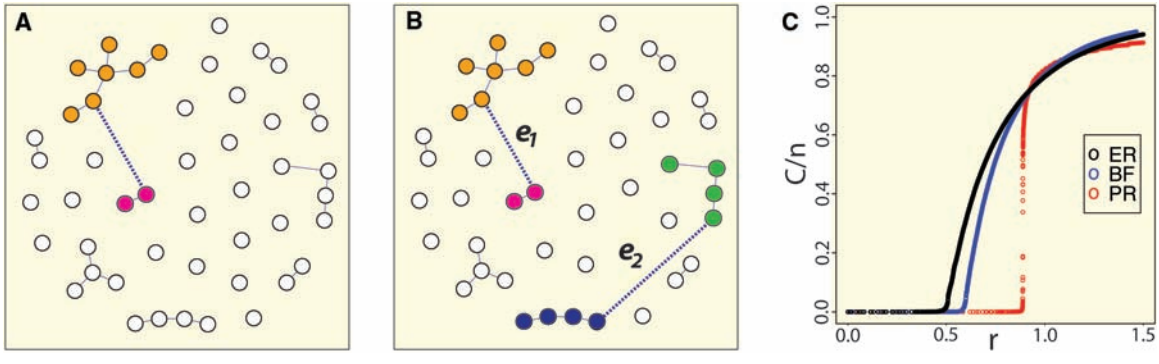

Fig. 1. Network evolution. (**A**) Under the Erdös-Rényi (ER) model, in each step two vertices are chosen at random and connected by an edge (shown as the dashed line). In this example, two components of size 7 and 2 get merged. (**B**) In models with choice, two random edges $\{e_1,e_2\}$ are picked in each step yet only one is added to the network based on some selection rule, whereas the other is discarded. Under the product rule (PR), the edge selected is the one minimizing the product of the sizes of the components it merges. In this example, e_1 (with product $2 \times 7 = 14$) would be chosen and e_2 discarded (because $4 \times 4 = 16$). In contrast, the rule selecting the edge minimizing the sum of the component sizes instead of the product would select e_2 rather than e_1. (**C**) Typical evolution of C/n for ER, BF (a bounded size rule with $K = 1$), and PR, shown for $n = 512{,}000$.